IIETA International Information and Engineering Technology Association
Advancing the World of Information and Engineering

Mathematical Modelling of Engineering Problems
Vol. 11, No. 11, November, 2024, pp. 2944-2952
Journal homepage: http://iieta.org/journals/mmep

Modeling of Composite Box Girder with Concrete—Corrugated Steel Webs of Base Plate

Maryam I. Jumaa*, Fareed H. Majeed

Civil Engineering Department, University of Basra, Basra 61004, Iraq

Corresponding Author Email: pgs.maryam.jumaa@uobasrah.edu.iq

https://doi.org/10.18280/mmep.111107

Received: 2 January 2024
Revised: 20 March 2024
Accepted: 30 March 2024
Available online: 29 November 2024

Keywords:
composite box girder, corrugated steel webs, shear connections, FE technique

ABSTRACT

The composite box girder with corrugated steel webs (CBGCSW) is a type of girder that has excellent properties, such as the lightness of the girders, a short construction period, optimum force distribution, good seismic performance, and an aesthetic appearance, which have promoted its use in bridges. However, it is difficult to predict its behavior under loads. In this research, non-linear finite element analysis (FEA) using the Abaqus software package was used to model different parts of the girder. The study aims to develop and improve the box girder in an economical way Through theoretical modeling built upon prior research, we assessed the alignment between experimental findings and theoretical analysis. Subsequently, we refined the model, integrating external stiffeners recognized for their ability to bolster the shear tolerance of the web alongside corrugated web structures. Leveraging the acknowledged benefits of this combination, our novel model demonstrated significantly heightened resilience compared to conventional designs lacking stiffeners, an 11% increase in resistance.

1. INTRODUCTION

CBGCSW is composed of a top concrete slab, corrugated steel webs, and a bottom plate. It is known for its ability to resist shear, flexural, and torsional stress while having fast construction and low cost compared to typical composite girders [1]. Chen et al. [2, 3] created two identical models, one with concrete-filled steel tubes and the other with hollow steel tubes, both of which exhibited high ductility and failed in a ductile manner. Concrete-filled steel tubes were found to enhance yield load and minimize deflection. The composite action between concrete and steel provides increased section modulus, resulting in higher resistance to bending and improved yield load capacity. Additionally, the concrete core contributes to reduced deflection by enhancing overall stiffness. Huang et al. [4] compared the two models to composite girders with truss chords and found that concrete-filling the chords reduced chord radial deformation and relieved hot-spot stress in composite girders by 18.5%-60.1%. It also decreased the rate of crack development during fracture propagation and failure and increased fatigue life by 61.5%. Ghanim et al. [1] explained that corrugated steel plate girders are widely used as a structural element in many sectors due to their beneficial qualities. They have a greater maximum moment carrying capacity than almost any hot-rolled section and transverse shear forces are transmitted only through the corrugated steel web. Webs with a greater depth-to-thickness ratio are typically used, which can lead to slender sections that are vulnerable to buckling on the flat web. However, advancements in the automated production process for corrugated steel webs and a reduction in weight have led to an increase in the use of corrugated web girders, particularly for wide-top flanged concrete box girders, so the using of corrugated webs prevent buckling occur when the section is slenderness. Tu et al. [5] presented a full-scale fatigue test and a numerical study of a new composite girder that was bent in four places. The test results showed that even at a relatively low level of stress, the composite girder still suffered fatigue damage at a very high number of cycles (9.84 million), causing it to fail as multiple cracks started at the top and bottom of the steel tube near the middle of the span and spread outward, here explain failure mode and crack propagation. He et al. [6] found that Live loads were effectively distributed using diaphragms, particularly under eccentric load conditions, because the diaphragms enhanced the lateral stiffness of two box girders joined together, so by connecting the girders, the diaphragms provided increased rigidity, ensuring that live loads were evenly spread across the structure. Zhou et al. [7] compared the original box girder design and proposed two improved CSW forms to increase transverse bending stiffness. The top flange is stiffened with transverse ribs, and lateral bracings are adjusted. These modifications aim to reduce the accumulated deformation differences caused by self-weight during segmental precasting using the short-line method. Numerical analysis further demonstrated that the improved structural form with lateral bracings reduced the maximum tensile transverse stress in the top concrete flange by 33% compared to the original box girder with CSWs. Ding et al. [8] found that the connection between the ultimate torsional strength and either the shear modulus or web thickness is almost linear. Under the same external torque, corrugated steel webs with a thick web can withstand higher torque than those with a thin web, it is clear from the above that the web thickness has an effective effect on the resistance to torsional torque. Majeed

[9] investigated the behavior of simply supported beams with lightweight concrete (LC) and normal concrete (NC) slabs. Shear interaction was considered at various levels (100% to 40%). It was discovered that the measured end slip for beams with LC had larger values for various degrees of shear connection than values obtained from testing on beams with NC. Al-Zaidee and Saadi [10] found a replace of concrete type for composite beam with a lightweight concrete deck slab, the strength and stiffness of the system are slightly impacted. The strength is only increased by 3.5% when normal weight concrete. Niu and Guo [11] found that many Multiple factors influenced the shear bearing capacity of girder oblique sections, including temperature, prestressed, material properties, and corrugated steel web thickness.

Finally, the above studies show the general behavior of composite girder with corrugated steel webs -concrete under different loads and finding weak points in the section for the possibility of improvement by adding strengthen to the weak sections.

2. AIM OF STUDY

The aim of this study is to investigate the static behavior of CBGCSW using finite element modeling. Since full-scale testing of CBGCSW can be costly and time-consuming, the use of FE modeling to determine the ultimate load and nonlinear response of such girders is a useful alternative. The study tests the validation of the FE model by comparing it to experimental test results. Additionally, the behavior of improving CBGCSW with vertical web stiffeners will be investigated. In general, it is difficult to estimate of CBGCSW using analytical methods, making the use of FE modeling a valuable tool in understanding their behavior. The form of stiffener's was chosen based on the that used in flat web. Thus, two effective elements of stiffeners can be combined with the corrugated web to produce a more efficiency model.

3. COMPOSITE BEAM DETAILS

Three CBGCSW specimens were modeled with simply supported clear span 2.5m (the dimensions were chosen to be suitable for the available testing device in anticipation of developing the work and conducting experimental modeling in the future). One of the specimens was modeled without additional vertical stiffeners (G0) as shown in the Figure 1, while the other two were with additional external stiffener plates (G30 and G50) to study the improvement in the behavior of the box girder with vertical stiffeners compared to one without it. Additionally, the effect of the width of the web stiffeners on the girder behavior was investigated by changing the stiffener width for specimens G30 and G50 with 30mm and 50mm respectively. Figure 1 shows the nominal geometry and details of a typical specimen and Table 1 shows the vertical stiffener details for the specimens. Studs were used as shear connections to tie the concrete slab to the top steel flanges.

Table 1. Detail of models

Specimen	Vertical Stiffeners Details		
	Thickness (mm)	Distance (mm)	Width(mm)
G0	0	-	0
G30	2	125	30
G50	2	125	50

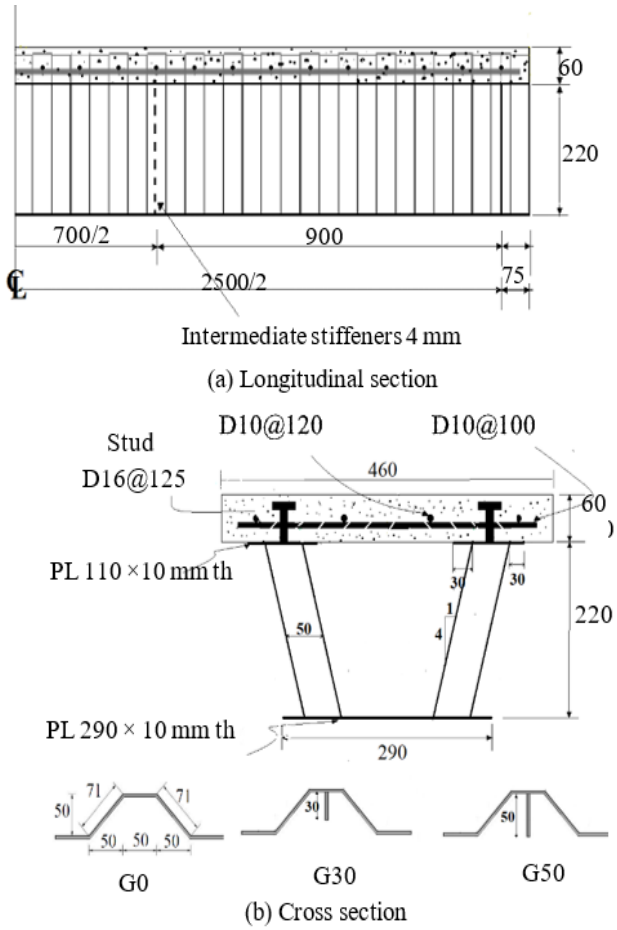

Figure 1. Nominal geometry of cross - section (all dimensions are in mm)

4. FINITE ELEMENT MODEL

The behavior and capacity of CBGCSWs were evaluated using a 3D nonlinear finite element model in ABAQUS 2020. The model incorporated flanges, a corrugated web, and a concrete flange, each simulated using a four-node doubly curved shell element with reduced integration (S4R) to accurately capture complex buckling behavior. To model concrete behavior, three alternative approaches were considered: the smeared cracking model, the brittle cracking model, and the concrete damaged plasticity (CDP) model. The CDP model was selected for its comprehensiveness as a continuum model, making it particularly suitable for characterizing concrete behavior in composite slab simulations. This model effectively captures the two primary modes of failure in concrete: crushing under compressive loads and tensile cracking. Figures 2 and 3 illustrate typical FEM components of the model, showcasing its structural integrity and strength.

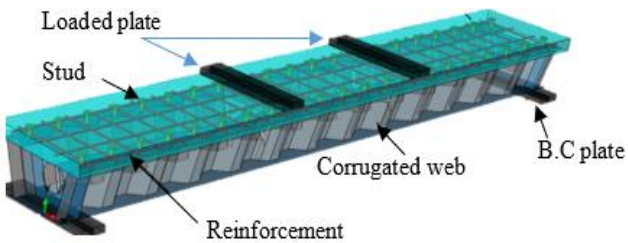

Figure 2. FEM for steel box specimens (model 1)

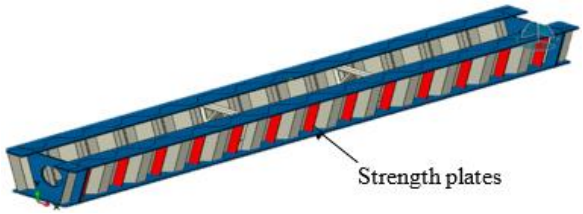

Figure 3. FEM for specimens (with strength)

5. MATERIAL PROPERTIES AND CONSTITUTIVE

5.1 Concrete

To simulate concrete part used solid element providing detailed stress distribution throughout the entire volume. Concrete behaves differently in compression and tension than steel reinforcement. According to the basic assumptions of CDP, there are two failure modes of the concrete material: tensile cracking and compressive crushing. The average compressive strength of concrete (f'_c) was 27.5 N/mm². Relations between f_c and f_{cu} are presented by Chen et al. [12], and the stress-strain curve of concrete shown in Figure 4. Table 2 shows the concrete properties for all models in this study.

$$f_c' = \begin{cases} 0.8f_{cu}, & f_{cu} \le 50\ Mpa \\ f_{cu} - 10, & f_{cu} > 50\ Mpa \end{cases}$$

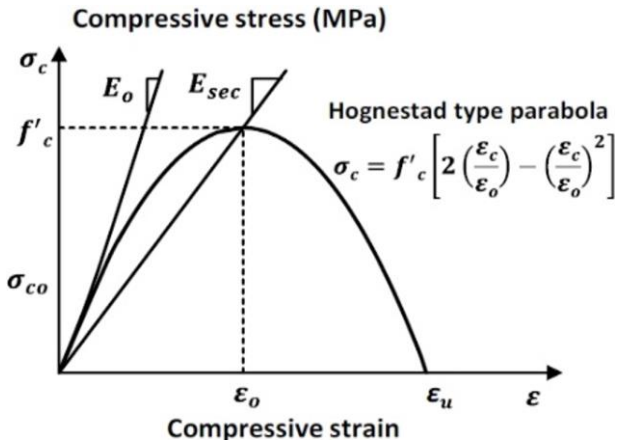

Figure 4. Stress-strain (compressive) curve of concrete

Table 2. Concrete properties

Mass Density Kg/mm³	Young's Modulus MPa	Compressive Strength f'c MPa	ε_o
2.4E_ 09	24647	27.5	0.002

Concrete damaged plasticity: The concrete damaged plasticity (CDP) model employs the Drucker-Prager plastic flow functional and Lubliner yield function to simulate the behavior of concrete under stress. This model is defined by five key parameters: the shape factor, eccentricity, the ratio of biaxial compressive stress to uniaxial compressive stress, dilation angle, and viscosity. These parameters are typically established through experimental measurements or by analyzing existing data.

Lubliner et al. [13] recommended a value of 2/3 for the shape factor and an eccentricity of 0.1, which approximates the ratio of uniaxial concrete compressive strength to tensile strength. As reported by Kupfer et al. [14], the ratio of biaxial compressive stress to uniaxial compressive stress for normal strength reinforced concrete is 1.16. The dilation angle, which indicates the internal friction angle of concrete, generally ranges from 31° to 42°. Demir et al. [15] suggested a viscosity parameter of 0.0005 to optimize numerical accuracy. Table 3 presents the data considered in this study.

Table 3. Factor of concrete properties

Dilation Angle	Eccentricity	fb0/fc0	K	Viscosity Parameter
31	0.1	1.16	0.667	0.0005

For compression behavior, the following data (Table 4) and Figure 5 are used.

Table 4. Stress-strain of compression behavior (concrete)

Stress (MPa) σ_c	Inelastic Strain ε_c^{in}
10	0
15.71685398	6.49839E-05
20.17747027	0.000145025
23.56721138	0.000266961
25.84087501	0.000431072
27.11891988	0.00064024
27.5	0.000884246
26.46090824	0.001421405
24.09757395	0.002021292
21.3448636	0.002633977
18.69744865	0.003236391
16.27352668	0.003838736
14.187811	0.00442436
7.700114836	0.007162584
4.675426178	0.009805305
3.123716348	0.012373262
2.236655657	0.014884252
1.670260181	0.017427233
1.295837673	0.019947424

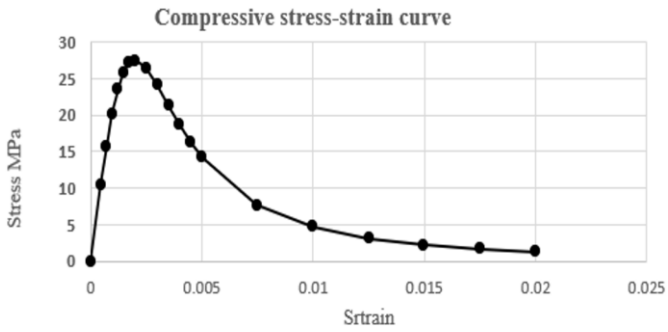

Figure 5. Compressive stress-strain curve (concrete)

For the tensile behavior, bilinear stiffening response is used, Gerwick Jr. [16] recommended the value to be the uniaxial cracking strength: f,cr=0.33√fc'. this is the value used to calibrate the tension stiffening curve by Hsu and Mo [17] as discussed earlier and the value used by Lee et al. [18] for peak tensile strength.

The fracture energy G_f is the fracture energy of concrete that represents the area under the tensile stress-crack displacement curve. The fracture energy G_f is related to the concrete's strength and aggregated size and can be calculated using Eq. (1) [19].

$$G_f = G_{f0}(f_{cm}/f_{cm0})^{0.7}(N/mm) \quad (1)$$

Gerwick Jr. [16] recommended the value to be the uniaxial.

Cracking strength: f,cr=0.33√fc', this is the value used to calibrate the tension stiffening curve by Hsu and Mo [17] as discussed earlier and the value used by Lee et al. [18] for peak tensile strength. Table 5 and Figure 6 are used in models.

The Hordijk 's model with two parameters, f_t and G_f:

$$\frac{\sigma(w)}{f_t} = \left[1 + \left(c_1 \frac{w}{w_{ult}}\right)^3\right] e^{\left(-\frac{c_2 w}{w_{ult}}\right)} - \frac{w}{w_{ult}}(1 + c_1^3)e^{-c_2} \quad (2)$$

where, c_1=3; c_2=6.93; and w_{ult}=5.136×$\boldsymbol{G_f}/f_t$.

Table 5. Stress-displacement of tensile behaviors (concrete)

Stress (MPa)	Displacement (mm)
3.042903097	0
1.649021782	0.066
0.779215604	0.173
0.629143257	0.22
0.458746567	0.308
0.395143878	0.35
0.338344875	0.39
0.284313161	0.43
0.22100944	0.48

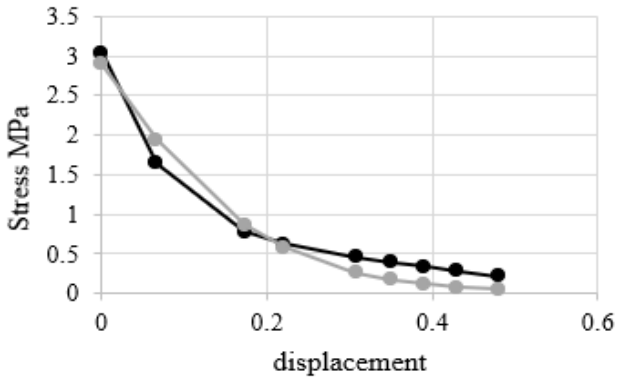

Figure 6. Tensile stress-displacement curve (concrete)

Compression damage: The compressive damage in concrete materials is quantified by the parameter d_c. A value of 0 for this parameter indicates that the concrete is undamaged, whereas a value of 1 signifies that the concrete is fully damaged. The damage parameter can be defined using a tabular format as shown in the following equation. If this parameter is not specified, the model defaults to functioning purely as a plasticity model.

$$\begin{aligned} b_c &= 0.7 \\ \varepsilon_c^{pl} &= b_c \varepsilon_c^{in} \\ d_c &= 1 - \frac{\sigma_c E_c^{-1}}{\varepsilon_c^{pl}\left(\frac{1}{b_c} - 1\right) + \sigma_c E_c^{-1}} \end{aligned} \quad (3)$$

where, d_c is the compression damage parameter, σ_c is the compression stress, and f_c' is the compressive strength of concrete. The compression damage used is shown in Table 6.

5.2 Steel reinforcement

The reinforcement in uniaxial tensile tests is characterized as a steel material based on experimental stress-strain results. The behavior of the steel is described using an elastic linear strain hardening bilinear curve. The elastic properties are defined by a longitudinal modulus of elasticity of 200 GPa and a Poisson's ratio of 0.3. According to the British Standards Institution, the plastic behavior is characterized by the actual stress, σs, and the true plastic strain, εspl. Table 7 presents the data used in determining the properties of the reinforcing bars.

5.3 Steel plate

The S4R element is chosen for its ability to model thin-shell plates, with high accuracy and computational efficiency.

The bi-linear plus nonlinear hardening model described by Eq. (4) below represents the rounded strain hardening response of hot-rolled steel and will therefore be suited for advanced numerical simulations of scenarios requiring tracking the progressive loss of stiffness. The nonlinear expression has a similar shape to that provided by Mander [20], and it has four model coefficients (K1, K2, K3, and K4) that are calibrated using least squares regression using tensile coupon test data. The authors believe that the quad-linear model is adequate and sufficiently accurate for the vast majority of engineering applications. Figure 7 shows stress-strain for steel plates in models.

Table 6. Compression damage

dc	Inelastic Strain
0	0
0.029665195	6.49839E-05
0.050463112	0.000145025
0.077284654	0.000266961
0.109803092	0.000431072
0.148620561	0.00064024
0.192084301	0.000884246
0.284277822	0.001421405
0.382797393	0.002021292
0.477107675	0.002633977
0.561377479	0.003236391
0.635592816	0.003838736
0.697500807	0.00442436
0.873063164	0.007162584
0.93941932	0.009805305
0.966984238	0.012373262
0.980081851	0.014884252
0.987203915	0.017427233
0.991290778	0.019947424

Table 7. Reinforcement stress

Ultimate Stress MPa	Plastic Pl Strain
560	0

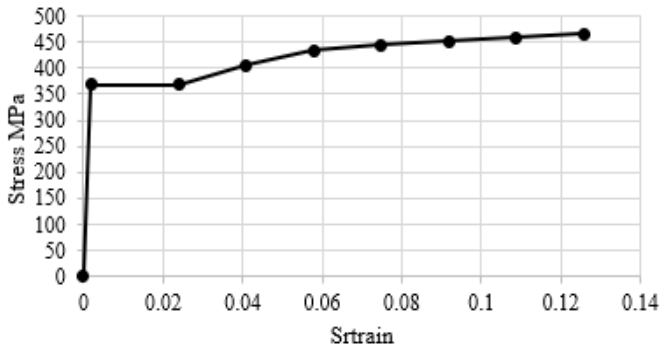

Figure 7. Stress -strain curve for steel plate

$$f(\varepsilon) = \begin{cases} E_\varepsilon & \text{for } \varepsilon \le \varepsilon_y \\ f_y & \text{for } \varepsilon_{sh} < \varepsilon \le \varepsilon_u \\ f_y + (f_u - f_y)\left\{ K_1\left(\dfrac{\varepsilon - \varepsilon_{sh}}{\varepsilon_u - \varepsilon_{sh}}\right) + \dfrac{K_2\left(\dfrac{\varepsilon - \varepsilon_{sh}}{\varepsilon_u - \varepsilon_{sh}}\right)}{\left[1 + K_3\left(\dfrac{\varepsilon - \varepsilon_{sh}}{\varepsilon_u - \varepsilon_{sh}}\right)^{K_4}\right]^{\frac{1}{K_4}}} \right\} & \text{for } \varepsilon_{sh} < \varepsilon \le \varepsilon_u \end{cases} \quad (4)$$

$\varepsilon_u = 0.6(1 - \frac{f_y}{f_u})$, but $\varepsilon_u \ge 0.06$ for hot − rolled steels

$\varepsilon_{sh} = 0.1\frac{f_y}{f_u} - 0.055$ but $0.015 \le \varepsilon_{sh} \le 0.03$

$A = \pi r^2$.

Finally, we summary the properties values used in models in Table 8.

Table 8. Properties of materials

Material		Properties	
Concrete		F_c'	27.5 N/mm^2
Reinforced steel		f_y	560 MPa
		f_u	670 MPa
Structural steel	Flange	yield strengths	418 MPa
		ultimate strengths	530 MPa
	Web	yield strengths	405 MPa
		ultimate strengths	528 MPa

6. INTERACTIONS

In the interaction module, you can specify mechanical interactions between different sections of a model or between a region and its surrounding environment. An example of such an interaction used in modeling is the contact between two surfaces. Additionally, other types of interactions like tie, embedded region, and coupling constraints can also be defined within this module. It is important to note that Abaqus/CAE does not automatically detect mechanical contact between part instances or regions of an assembly based on proximity alone; such interactions must be explicitly defined in the Interaction module. Interactions are step-dependent objects, meaning that their active phases during the analysis must be specified. Table 9 and Figure 8 provide a summary of interactions for all models.

Table 9. Interaction for all model

No.	Interaction	Master Surface	Slave Surface
1	Surface to surface contact	Top steel flanges	Bottom surface of concrete slab
2	Surface to surface contact	Top loaded plate	Top slab surface
3	Embedded region constrains	Reinforcement bars +studs (Embedded region)	Concrete slab (host region)
4	Tie constrain	Bottom flange	Bottom plate
5	Tie constrain	Base of studs	Top flange
6	Coupling constrains	Reference point load 3	Middle of line nodes for loaded plate

Note: The interaction numbers are indicated in Figure 8 to illustrate the interaction surfaces.

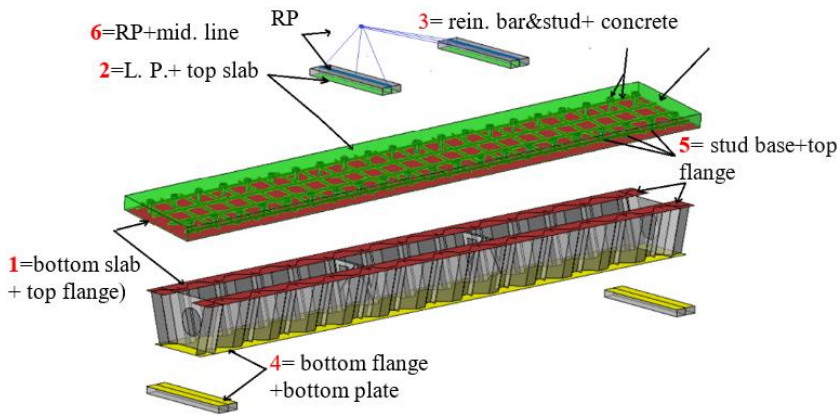

Figure 8. Interaction surfaces for model

7. VERIFICATION ANALYTICAL MODEL

Hassanein et al. [20] offered experimental work as shown in Figure 9 investigations to evaluate the shear and bending moment behavior of a composite box girder with steel corrugated webs. We study the experimental work by finite element analytical in ABAQUS 2020 by using the same data in his work and compared the results. Figure 10 views the FEM for box girder.

The load-mid span deflection and failure mechanisms based on experimental testing were compared to finite element findings. As demonstrated in Figure 11, the finite element findings accord well with the experimental data. The finite element analysis predicted the maximum load for the specimen, which was 1090 kN, while the highest experimental load for the verification specimen was 1055 kN.

According to Hassanein, the effective width for shear resistance of a concrete slab is roughly equal to the width of the upper steel flange. Figure 12 depicts the von Mises stress levels at failure of specimen. The stresses can be seen to be

focused in the upper and lower flanges, at the plastic hinge locations, and in the web yielded zone. Figure 13 also depicts the normal stress contours at failure of specimen. Normal stresses are similarly focused with high values at the plastic hinge sites in the upper and lower flanges.

As shown in Figure 14, the cracks are localized at shear stud positions and are restricted by the upper steel flange band width, after which the cracks progress throughout the whole width of the slab.

Figure 9. Specimen fabrication from the study conducted by Hassanein et al. [20]

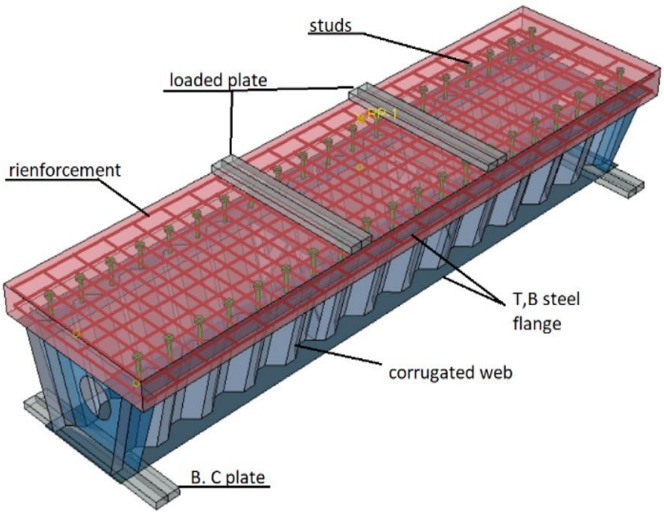

Figure 10. Detail of FEM box girder

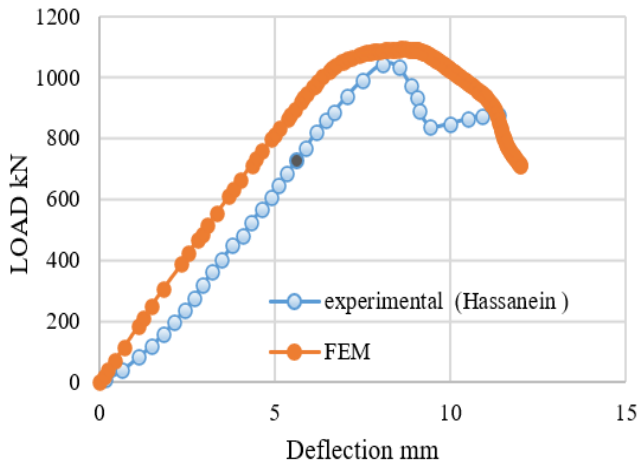

Figure 11. Load-deflection curve for exp. (Hassanein) and FEA

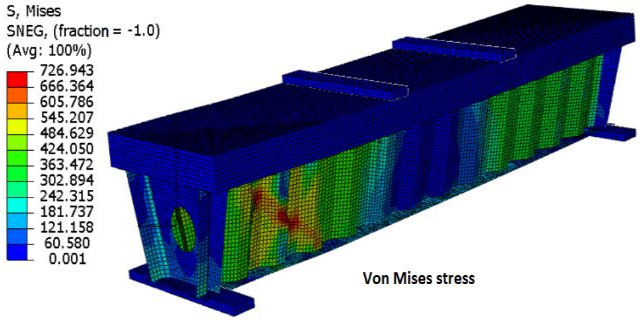

Figure 12. The von Mises stress

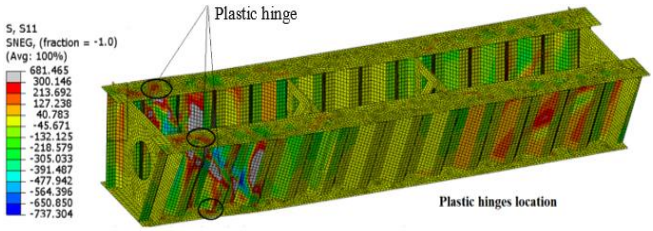

Figure 13. Normal stresses at failure

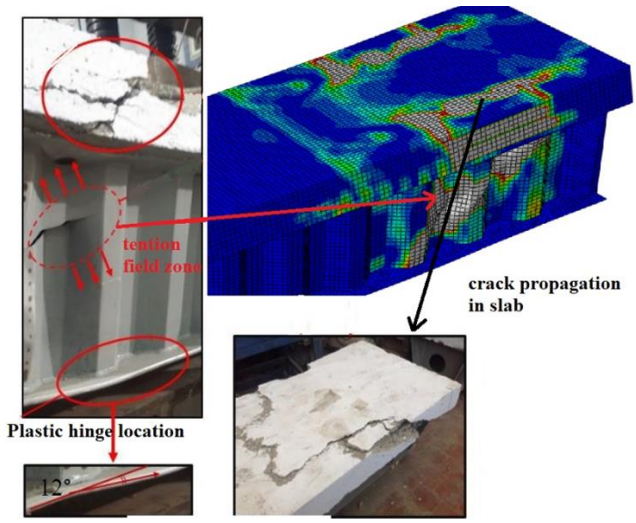

Figure 14. Failure mechanisms, both experimental (Hassanein) and FEA

8. RESULTS AND DISCUSSIONS

After applying test loads (2-point load) to simulate real-world vehicle wheel movements on girder beams, it is evident that the incorporation of external support for the web significantly influences the structural performance. The results underscore this impact with detailed load values and deflections for different models:

Model 1 (G0), the ultimate load reached 568.550 kN with a corresponding deflection of 14 mm.

Model 2 (G30), featuring a 30 mm width strength plate, exhibited an ultimate load of 576.455 kN and a deflection of 16 mm.

Model 3 (G50), with a 50 mm width strength plate, significantly improved, showing an ultimate load of 632.066 kN and a deflection of 54 mm.

The ultimate load increased by 11.17% in Model 3 (G50) due to the application of a 50 mm strength plate in the web and by 1.4% in Model 2 (G30). Model 3 also exhibited increased

ductility, as evidenced by the higher mid-beam deflection values.

The load-deflection relationships are detailed in Figure 15, while Table 10 summarizes these results. The addition of strength plates (stiffeners) not only enhanced the load-bearing capacity but also reduced shear stress, which typically leads to failure, as depicted in Figures 16 and 17. In box beams, the thicker flanges are more resistant to buckling, whereas the webs are more prone to local buckling due to shear, transverse compression loads, such as those from a bearing reaction, or longitudinal compression stresses from bending. The presence of stiffeners significantly enhances resistance to local buckling in all scenarios.

Furthermore, the finite element model predictions for concrete slab crack growth and crushing are illustrated in Figure 18, clearly displaying the fracture patterns from the finite element models. This visualization helps in understanding the effectiveness of the model improvements and the dynamic response of the structure under load.

The yield area started in the web and thus expanded as a tension area that determined it from the lower and upper flanges, where the concrete and the studs are present, and the bearings act as a stabilizer for the upper flange, which bends down as a result of the effect of the tension area, so the crack focus in stud location and extends in the slab area is determined by the width of the upper flanges. All cracks were reported to have occurred along the stiffener-to-flange line. Furthermore, no fractures developed at the web-to-flange weld in the stiffened beams. It is worth noting that both the unstiffened and stiffened beams exhibit distortional lateral buckling, while the unstiffened beam buckles laterally with significant web distortion.

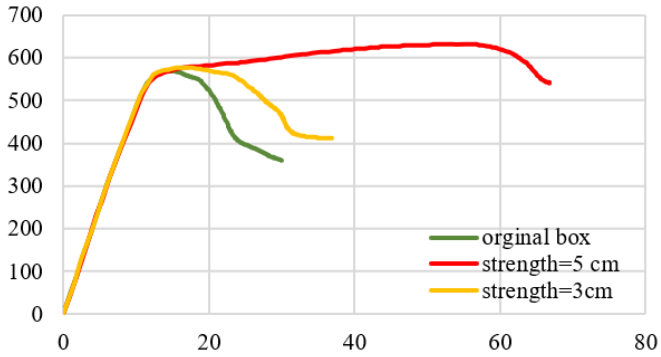

Figure 15. Load-deflection curve for three model

Table 10. Final result for models

No.	Models	F_u (ABAQUS) kN	F_u (exp.) [20] kN	Deflection mm	Convergence Ratio%
1	Hassanein et al. [21]	1091	1044	8	95%
2	G0	568.550	-	14	-
3	G30	576.455	-	16	-
4	G50	632.066	-	54	-

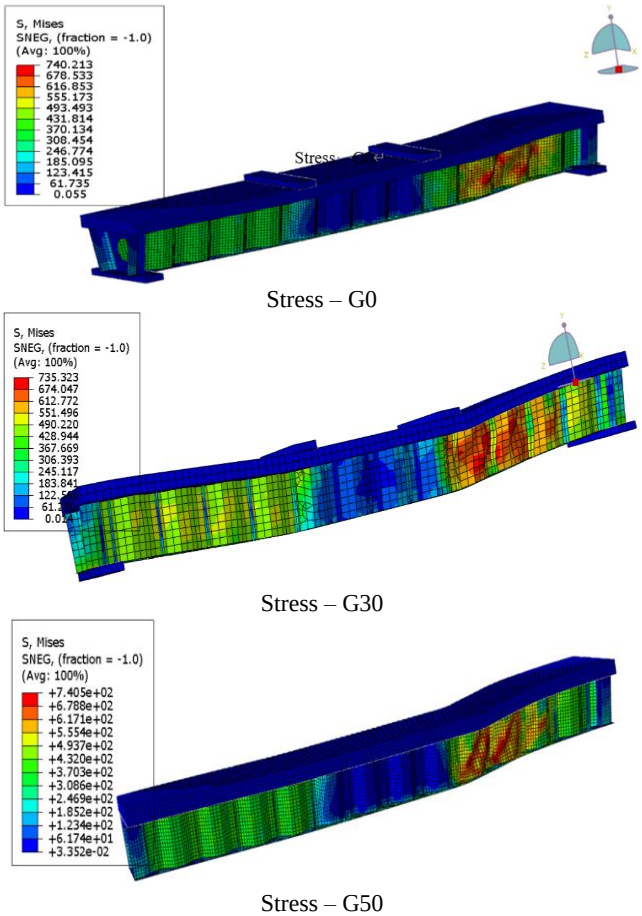

Figure 16. Stress (S12) for models

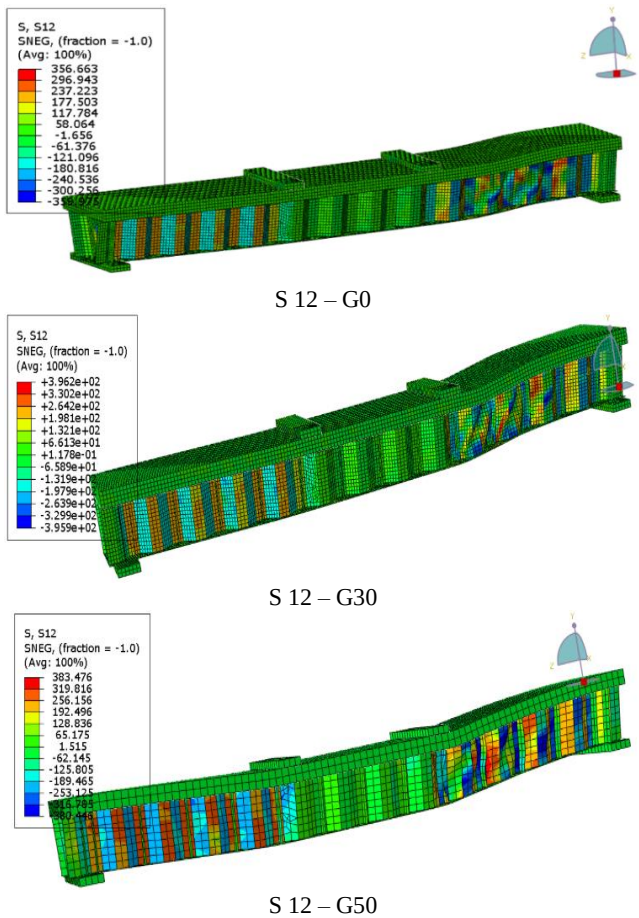

Figure 17. Stress (von- Mises) for models

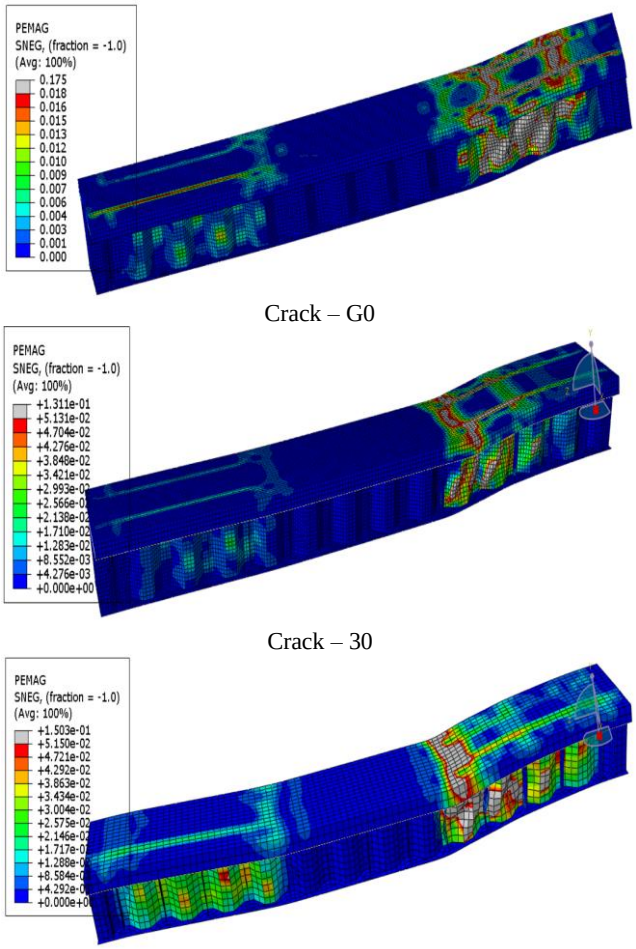

Figure 18. Cracks for all models

9. CONCLUSIONS

In this work, composite box girders with corrugated steel web underwent finite element analysis to examine their bending and shear behaviour with strengthening. From this research, the following findings are drawn:

-The steel corrugated webs on the composite box girders with strengthens have a sufficiently ductile behaviour.

-By preventing the predicted rapid collapse of the corrugated web, the concrete slab helps to improve the shear behaviour of steel box girders with corrugated web.

-Because steel is supposed to transmit shear and concrete is expected to withstand bending most of the time, the materials are used more effectively.

-The ductility of model G50 resulted in a notable increase in buckling wave compared to model G0, owing to its wider plasticity range before failure

-The employ the strengthen decrease the shear stress in web.

-The model gave a very good representation of the behavior of the actual model with a percentage of approximately 95%.

Future studies could build upon the findings of this research in several ways to address remaining questions and explore related issues:

Experimental validation: Performing experimental validation of the findings using physical testing of box girder prototypes. This can verify the accuracy and applicability of the theoretical models developed in this study

Cyclic loads: Cyclic loads can be applied, which represent, for example, the movement of vehicles over the bridge to understand the behavior of the box girder more realistically.

REFERENCES

[1] Ghanim, G., Baldawi, W.S., Ali, A.A. (2021). A review of composite steel plate girders with corrugated webs. Engineering and Technology Journal, 39(12): 1927-1938. http://doi.org/10.30684/etj.v39i12.2193

[2] Chen, Y., Dong, J., Tong, Z., Jiang, R., Yue, Y. (2020). Flexural behavior of composite box girders with corrugated steel webs and trusses. Engineering Structures, 209: 110275. https://doi.org/10.1016/j.engstruct.2020.110275

[3] Chen, Y., Dong, J., Xu, T. (2018). Composite box girder with corrugated steel webs and trusses–A new type of bridge structure. Engineering Structures, 166: 354-362. https://doi.org/10.1016/j.engstruct.2018.03.047

[4] Huang, H., Chen, K., Wu, Q., Nakamura, S. (2022). Fatigue performance test and numerical analysis of composite girders with CSW-CFST truss chords. Applied Sciences, 12(11): 5459. https://doi.org/10.3390/app12115459

[5] Tu, B., Cai, S., Li, J., Liu, H. (2021). Fatigue assessment of a full-scale composite box-girder with corrugated-steel-webs and concrete-filled-tubular flange. Journal of Constructional Steel Research, 183: 106768. https://doi.org/10.1016/j.jcsr.2021.106768

[6] He, J., Liu, Y., Wang, S., Xin, H., Chen, H., Ma, C. (2019). Experimental study on structural performance of prefabricated composite box girder with corrugated webs and steel tube slab. Journal of Bridge Engineering, 24(6): 04019047. https://doi.org/10.1061/(ASCE)BE.1943-5592.0001405

[7] Zhou, M., Liu, Y., Deng, W., Hassanein, M.F., Zhang, H. (2019). Transverse analysis of full-scale precast segmental box girder segments with corrugated steel webs: Experimental tests and FE modelling. Engineering Structures, 187: 231-241. https://doi.org/10.1016/j.engstruct.2019.02.072

[8] Ding, Y., Jiang, K., Liu, Y. (2012). Nonlinear analysis for PC box-girder with corrugated steel webs under pure torsion. Thin-Walled Structures, 51: 167-173. https://doi.org/10.1016/j.tws.2011.10.013

[9] Majeed, F.H. (2018). Behavior of steel-lightweight concrete composite beams with partial shear interaction. Journal of University of Babylon for Engineering Sciences, 26(2): 20-34.

[10] Saadi, T.H., Al-Zaidee, S.R. (2022). Finite element modeling of partially composite light-gage steel tube beam with lightweight concrete deck slab. Mathematical Modelling of Engineering Problems, 9(2): 515-522. https://doi.org/10.18280/mmep.090230

[11] Niu, Q.C., Guo, X.H. (2023). Application of a thermodynamic model in durability analysis of bridge structures under climatic variability. International Journal of Heat and Technology, 4(4): 901-909. https://doi.org/10.18280/ijht.410412

[12] Chen, Z.Y., Zhu, J.Q., Wu, P.G. (1992). High Strength Concrete and Its Application. Tsinghua University Press, Beijing, China.

[13] Lubliner, J., Oliver, J., Oller, S., Onate, E. (1989). A plastic-damage model for concrete. International Journal

of Solids and Structures, 25(3): 299-326. https://doi.org/10.1016/0020-7683(89)90050-4
[14] Kupfer, H., Hilsdorf, H.K., Rusch, H. (1969). Behavior of concrete under biaxial stresses. Journal Proceedings, 666(8): 656-666. https://doi.org/10.14359/7388
[15] Demir, A., Ozturk, H., Edip, K., Stojmanovska, M., Bogdanovic, A., Seismology, E. (2018). Effect of viscosity parameter on the numerical simulation of reinforced concrete deep beam behavior. Journal of Science and Technology, 8(3): 50-56.
[16] Gerwick Jr., B.C. (1997). Construction of Prestressed Concrete Structures. John Wiley & Sons.
[17] Hsu, T.T., Mo, Y.L. (2010). Unified Theory of Concrete Structures. John Wiley & Sons.
[18] Lee, S.C., Cho, J.Y., Vecchio, F.J. (2013). Tension-stiffening model for steel fiber-reinforced concrete containing conventional reinforcement. ACI Structural Journal, 110(4): 639-648.
[19] Comité Euro-International du Béton. (1993). CEB-FIP Model Code 1990: Design code. Thomas Telford Publishing.
[20] Mander, J.B. (1983). Seismic design of bridge piers. PhD thesis, University of Canterbury.
[21] Hassanein, S.A., Salem, E.S., Mohmoud, A.M. (2018). Shear behavior and capacity of composite box girder with steel corrugated web. Al-Azhar University Civil Engineering Research Magazine, 40(3): 33-48. https://www.azharcermjournal.com/CERMF1807/P18-07-04.pdf.

NOMENCLATURE

c_1	constant 1
c_2	constant 2
d_c	the compression damage parameter
E_c	modulus of elasticity of concrete
Es	modulus of elasticity of reinforcement and structural steel
E_{sh}	strain hardening modulus
f_{cm}	mean compressive strength of concrete MPa
f'_c	specified compressive strength of concrete
f_{cmo}	reference value for compressive strength of concrete MPa
f_s	stress in the steel
f_t	maximum tensile strength of the concrete MPa
f_y	specified yield strength for reinforcement concrete
G_f	fracture energy
G_{f0}	base value of fracture energy
h	height or depth of member
I	moment of inertia of section about centroidal axis
$K1$, $K2$, $K3$, $K4$	coefficients which are calibrated herein based on tensile coupon test data by means of least squares regression
ℓ	span length of beam
n	modules of elasticity transformation coefficient for steel to concrete
s	center-to-center spacing of reinforcement mm
t_f	thickness of flange mm
t_w	thickness of the web mm
w	is the crack width mm
w/cm	water-cementitious material ratio
w_{ult}	the critical crack width at which the crack is stress free mm

Greek symbols

ε_c^{el}	elastic strain in concrete
ε_c^{in}	inelastic strain in concrete
ε_c^{pl}	plastic strain in concrete
ε_s	strain in the steel
ε_c	compressive strain in concrete
ε_{sh}	strain hardening strain
ε_u	ultimate strain in concrete
ρ	ratio of as to bd
μ	coefficient of friction